Electronic Supplementary Information, ESI

A diamantane-4,9-dicarboxylate based UiO-66 analogue: challenging larger hydrocarbon cage platforms

Vasily Gvilava,[a] Maximilian Vieten,[a] Robert Oestreich,[a] Dennis Woschko,[a] Moritz Steinert,[a] Ishtvan Boldog,*[a] Roman Bulánek,[b] Natalie A. Fokina,[c] Peter R. Schreiner[c] and Christoph Janiak*[a]

[a] Institut für Anorganische Chemie und Strukturchemie, Heinrich-Heine-Universität Düsseldorf, Universitätsstr. 1, D-40225 Düsseldorf, Germany.E-mail: janiak@uni-duesseldorf.de
[b] Department of Physical Chemistry, Faculty of Chemical Technology, University of Pardubice, Studentska 573, 532 10 Pardubice, Czech Republic
[c] Institut für Organische Chemie der Justus-Liebig-Universität Gießen, Heinrich-Buff-Ring 17-19, 35392 Gießen, and Center for Materials Research (ZfM), Heinrich-Buff-Ring 16, 35392 Gießen, Germany

E-mails: vasily.gvilava@hhu.de, mavie107@uni-duesseldorf.de, Robert.Oestreich@hhu.de, dennis.woschko@hhu.de, Moritz.Steinert@gmx.de, boldogi@hhu.de, Roman.Bulanek@upce.cz, nfokina@gmx.de, prs@uni-giessen.de, janiak@uni-duesseldorf.de

Contents

S1 Synthesis

Materials. $ZrCl_4$ (97+%, Acros Organics), $ZrOCl_2 \cdot 8H_2O$ (99%, Sigma-Aldrich), diamantane-4,9-dicarboxylic acid (H_2L) (TransMIT chemicals), N,N-dimethylformamide (DMF; 99.8%, Honeywell), formic acid (99%, Sigma-Aldrich), deionized water.

General method of synthesis:
The synthetic optimization studies of HHUD-3 involved the use of both $ZrCl_4$ and $ZrOCl_2 \cdot 8H_2O$ (the respective optimized samples are given as **2.1** and **2.2**, respectively). It was shown that at least near the optimal conditions the crystallinity as witnessed by the PXRD patterns, and gas sorption data are very close, demonstrating an only minor influence of the metal source.

$ZrCl_4$ or $ZrOCl_2 \cdot 8H_2O$ and diamantane-4,9-dicarboxylic acid were suspended in DMF. Formic acid was added as modulator (see Table S1 for details). The mixture was homogenized by thorough shaking (no clear solution formed under room temperature, just under heating). The turbid suspension was hermetically sealed in a threaded culture tube with a PTFE-lined screw cap. The sealed tube was heated at 120 °C for 72 h with 2 h of heating and cooling ramps, respectively. After cooling, the product was separated by centrifugation and washed two times with DMF and two times with ethanol. It was dried in air for 48 h and subsequently at 80 °C for another 24 h. In order to prepare larger amount of the product, parallel syntheses were used.

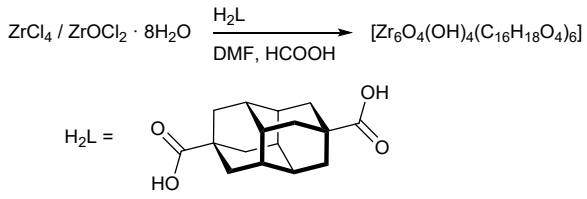

diamantane-4,9-dicarboxylic acid

Synthesis of **1** ($Zr_6O_4(OH)_4(C_{16}H_{18}O_4)_6$): 16 mg (0.07 mmol) of $ZrCl_4$ and 21 mg (0.08 mmol) of diamantane-4,9-dicarboxylic acid suspended in 8 mL of DMF with 0.2 mL of formic acid being added afterwards. The mixture was homogenized and sealed in a 10 mL culture tube and heated at 120 °C for 72 h with 2 h of heating and cooling ramps respectively. The formed white precipitate was separated by centrifugation and washed two times with 5 mL of DMF and two times with 5 mL of ethanol. It was dried in air for 48 h and subsequently at 80 °C for another 24 h.
Yield: 17 mg (~66%).[A].

Synthesis of **2.1 / 2.2** ($Zr_6O_4(OH)_4(C_{16}H_{18}O_4)_6$): 7 mg (0.03 mmol) of $ZrCl_4$ (**2.1**) or 10mg (0.03 mmol) of $ZrOCl_2 \cdot 8H_2O$ (**2.2**) and 22 mg (0.08 mmol) of diamantane-4,9-dicarboxylic acid were suspended in 8 mL of DMF, followed by the addition of 0.2 mL of formic acid. The mixture was homogenized and sealed in a culture tube (diameter of ~14 mm), were used. An attempted scale-up using tubes with larger volume led to a decrease in the number of successful syntheses. The sealed tubes were heated at 120 °C for 72 h with 2 h of heating and cooling ramps respectively. The formed white precipitate was separated by centrifugation and washed two times with 5 mL of DMF and two times with 5 mL of ethanol. It was dried in air for 48 h and subsequently at 80 °C for another 24 h. Yield: 8 mg (~63%)[A] (**2.1**) / 9 mg (~70%)[A] (**2.2**)

Synthesis of **3** ($Zr_6O_4(OH)_4(C_{16}H_{18}O_4)_6$): 10mg (0.03 mmol) of $ZrOCl_2 \cdot 8H_2O$ and 11 mg (0.04 mmol) of diamantane-4,9-dicarboxylic acid were suspended in 2 mL of DMF and 0.05 mL of formic acid was added to the suspension. The mixture was homogenized and sealed in a culture tube (tube diameter ~14 mm) and heated at 120 °C for 72 h with 2 h of heating and cooling ramps respectively. The formed gel-like precipitate was separated by centrifugation and washed two times with 5 mL of DMF and two times with 5 mL of ethanol. It was dried in air for 48 h and subsequently at 80 °C for another 24 h to yield 7 mg (~60%)[A] of a white powder.

Table S1 Reaction parameters for the synthesis of HHUD-3

Sample	{Zr} source	Amount of {Zr} [a] [mg] / [mmol]	Amount of H_2L [a] [mg] / [mmol]	DMF [mL]	HCOOH [mL]
1	$ZrCl_4$	16 / 0.07	22 / 0.08	8	0.2
2.1	$ZrCl_4$	8 / 0.03	22 / 0.08	8	0.2
2.2	$ZrOCl_2 \cdot 8H_2O$	10 / 0.03	22 / 0.08	8	0.2
3	$ZrOCl_2 \cdot 8H_2O$	10 / 0.03	11 / 0.04	2	0.2

[a] {Zr} is the used zirconium salt, H_2L is diamantane-4,9-dicarboxylic acid

[A] Percentage yield refers to the ideal formula and molecular weight of the non-defective compound without guest molecules.

S2 Structural analysis of HHUD-3: Rietveld refinement of PXRD data

Powder X-ray diffraction (PXRD) patterns were measured for sample **1** of HHUD-3 over the 2θ range of 2–100° using a Rigaku MiniFlex600 diffractometer (600 W, 40 kV, 15 mA source) in reflective mode, equipped with a Bragg-Brentano goniometer, graphite monochromator and HyPix-400 MF 2D hybrid pixel array detector (HPAD). The measurement was performed at room temperature with 0.01° steps using Cu-Kα radiation (λ = 1.54182 Å).

Powder X-ray diffraction (PXRD) patterns

The PXRD pattern of **1** (Fig. S1) bears evident similarity to the simulated patterns for the **fcu** structures of UiO-66 and UiO-67. The observed peak shifts suggest that the cell parameters for **1** are between the ones for UiO-66 and UiO-67, in accordance with the relative length of the ligands (1,4-benzenedicarboxylate < diamantane-4,9-dicarboxylate < 4,4'-biphenyldicarboxylate). The comparison of the PXRD patterns for the different HHUD-3 samples shows a good peak-position matching, however **3** features peaks with broader reflections, which is regarded as a consequence of lower crystallinity and smaller particle sizes.

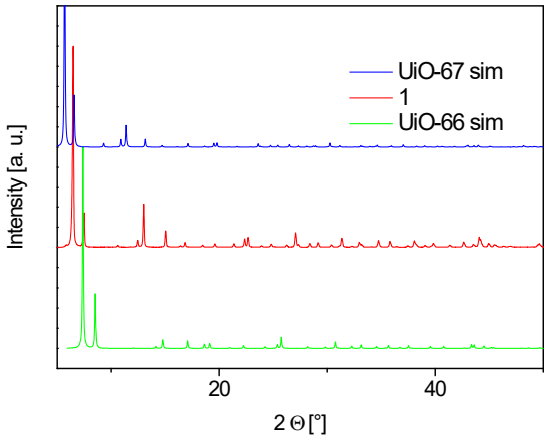

Fig. S1 Powder X-ray diffractogram of HHUD-3 sample **1** in comparison to simulated X-ray diffractograms of UiO-66[1] and UiO-67.[2]

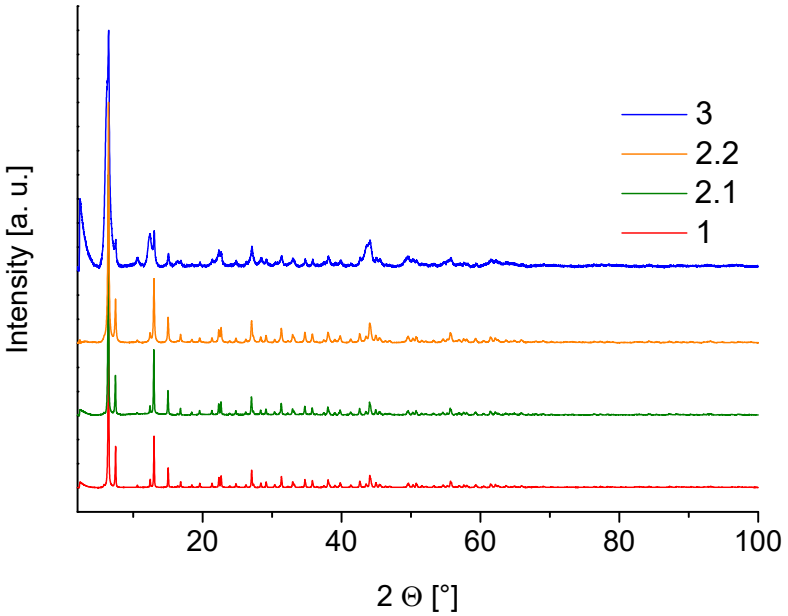

Fig. S2 Powder X-ray diffractograms of samples **1**, **2.1**, **2.2** and **3** of the HHUD-3 material, synthesized under different conditions.

Rietveld refinement

The sample was partially degassed (120 °C, 10^{-2} Torr); the procedure leaves a significant amount of the solvent in the pores, but the sample retained a high level of crystallinity. The measurement was performed using a Rigaku Miniflex PXRD diffractometer using monochromated Cu-Kα radiation (λ = 1.54182 Å) on a flat sample using a low-background silicon sample-holder with an indent. The sample was thoroughly homogenized, but no special grounding or sieving were used. The measurement was performed in air; a repeated measurement confirmed the stability of the sample at least during the time of the measurement (~11 h).

The indexing performed by GSAS-II suite[3] listed both *P*m3̄m and *F*m3̄m as space groups. The primitive centering could indicate the presence of a superlattice with correlated missing cluster defects or an admixture of a pure phase corresponding to **reo** topology.[4] However, the h+k, k+l or h+l = 2n+1, which are systematically absent for the F-centering are non-discernible, (Fig. **S3**). The weak low-angle peaks characteristic for the **reo** structure of UiO-66,[4] which should be observed for 2θ < 6°, are absent (that does not mean that the missing cluster defects are missing, but that they are not regular enough to give a clear contribution to the PXRD pattern). The refinement was performed in the *F*m3̄m space group.

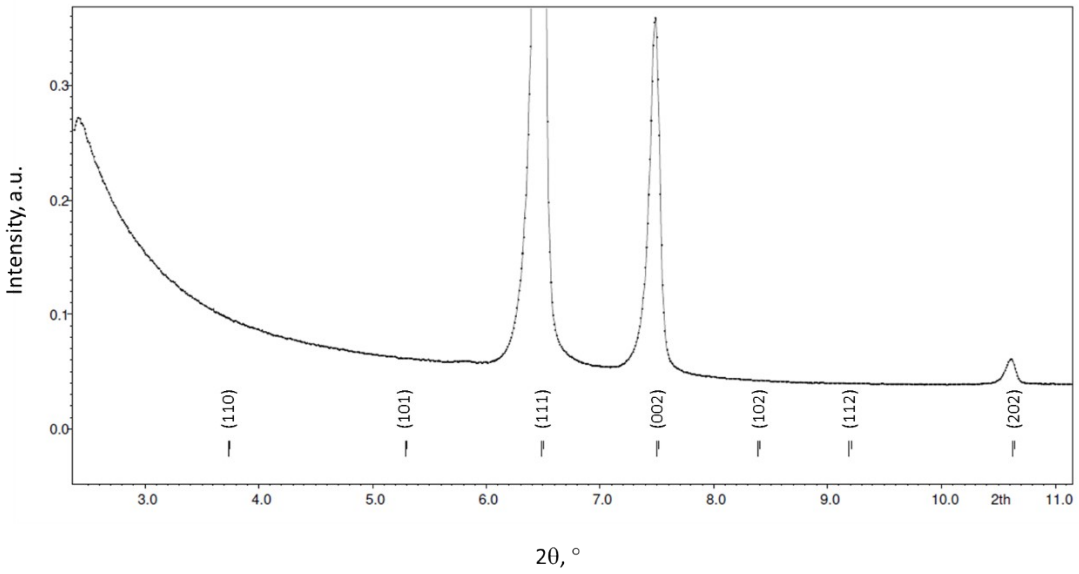

Fig. S3 Expansion of the low angle region of the PXRD pattern for **1**. The intensities of the h+k, k+l or h+l = 2n+1 reflections, which are systematically absent for the F-centering, are not discernible.

The initial idealized structural model of a UiO-66 type compound was constructed geometrically, using standard interatomic bond lengths and angles. The *F*m3̄m symmetry demands an *m.mm* site symmetry and the diamantane moiety (D_{3d}) was modelled as disordered over two positions, related through an inversion center (D_{6h} symmetry compatible with the site symmetry).

The Rietveld refinement was performed using the Jana 2006 software, v20151025 [5] (see Table S2 for summary).

The next general parameters were refined freely: the background (36 Legendre polynomials), the unit cell edge length, peak shape (Pseudo-Voigt, four parameters), peak asymmetry correction by divergence (HpS/L), focusing correction for Bragg-Brentano geometry, and the sample level shift parameter (one parameter for each case, if not indicated otherwise).

The coordinates of the Zr, O atoms and carbon atoms belonging to the non-disordered part of the ligand were refined freely. The site sharing of the μ_3-O/OH ligands was resolved explicitly. The disordered part of the diamantanedicarboxylate ligand was readjusted geometrically after initial convergence and was kept fixed. The occupancy factor of the diamantane moiety was refined (it was assumed that the positions representing the missing ligands are completed by carboxylate ligands, which is exact for the missing ligand defects), which ostensibly improved the fit (~1+% R_p); a site-occupancy factor, SOF of 0.74 was found, which corresponds to 0.76*6 = ~4.6 of the diamantanedicarboxylate linkers, with the rest belonging to formate ligands (two terminal formate ligands replace one bridging dicarboxylate linker). Accordingly, the formula $[Zr_6O_4(OH)_4(C_{16}H_{18}O_4)_{4.6}(HCOO)_{2.8}]$ was ascribed, based solely on the PXRD refinement (the number of defects, determined *via* that approach, is highly imprecise. It is the more so because the guest molecules were also modeled and their refinement is to some extent correlated with the refinement of the number of defects). The guest molecules were modeled by oxygen atoms, which were refined freely regarding both coordinates and occupancies. The final cycles of refinement were performed with fixed occupancies of the guest molecules to improve convergence at low parameter-shift values.

The thermal displacement parameters were refined separately for the Zr1 atom in an anisotropic model (two independent parameters, accounting for the site symmetry) and for all other atoms in an isotropic model, keeping the values for the latter equal. In all cases an isotropic approximation was used except for Zr1.

Table S2 Rietveld structure refinement data for $[Zr_6O_4(OH)_4(C_{16}H_{18}O_4)_{4.6}(HCOO)_{2.8}]$, **1**.

	1
Empirical formula	$C_{75.8}H_{82.1}O_{32.0}Zr_6$ $[O_{6.3}]$ [a]
M_r /g mol^{-1}	2052.7
T /K	295
Diffractometer	Rigaku MiniFlex [b]
Wavelength /Å [b]	1.54051, 1.54433 (Cu Kα_1, Kα_2) [c]
Crystal system	Cubic
Space group	$Fm\bar{3}m$
a /Å	23.49022(13)
V /Å^3	12961.68(12)
Z	4
Calc. density /g cm^{-3}	1.1048 [1.0529, no guests]
μ /mm^{-1}	4.331
F(000)	4339
θ range (refinement) /°	5.00 to 99.99°
θ step /°	0.01
Parameters / restraints/ constraints	59 / 1 / 52
R_p, wR_p	0.0315, 0.0450
R[|F|>2σ(|F|)], wR [d]	0.0346, 0.0508
R, wR (all data) [d]	0.0346, 0.0508
Largest diff. peak and hole /eÅ^{-3}	0.30, -0.26
Goodness of fit, χ^2 [e]	5.90

[a] The ascribed molecular formula corresponds to $[Zr_6O_4(OH)_4(C_{16}H_{18}O_4)_{4.56}(HCOO)_{2.86}]$, where the 4 H atoms of μ_3-OH and the H atoms of the formate ligands were not refined, hence for the calculation of the empirical formula and the molar mass M_r the formula is $[Zr_6O_4(O)_4(C_{16}H_{18}O_4)_{4.56}(COO)_{2.86}]$. The 6.3 O atoms given in brackets separately correspond to the modeled guest molecules and are not included in the molar mass M_r. Further, the formula assumes a missing linker defect model (an approximation in this case). The general formula with formate as a modulator, which substitutes a part of the bifunctional ligand is $[Zr_6O_4(OH)_4(C_{16}H_{18}O_4)_y(HCOO)_x]$, where $0.5x + y = 6$ and $x \leq 4$. The value x = 0 corresponds to a defect-free UiO-66 analogue, $[Zr_6O_4(OH)_4L_6]$. The value x = 4 is the maximal reasonable number of defects. The value of x was refined freely.

[b] 600 W X-ray tube, 'D/teX Ultra' solid-state (silicon) strip detector, Benchtop Bragg-Brentano geometry.

[c] The ratio was not refined or established independently, but taken as $I(K_{\alpha 2})/(K_{\alpha 1}) = 0.497$

[d] Based on extracted structure factors (synonyms: R_{Bragg}, R_F).

[e] The goodness of fit or χ^2 in PXRD refinement is $\chi^2 = \frac{\sum_{i=1}^{n} w_i \left(Y_i^{obs} - Y_i^{calc}\right)^2}{n-p}$, where n is the total number of measured data points; p is the number of free least squares parameters; Y_i^{obs} is the observed intensity of the i-th data point; Y_i^{calc} is the calculated intensity of the i-th data point; w_i is the weight of the i-th data point, which is usually taken as $w_i = 1/\sigma^2 = 1/Y_i^{obs}$.[6]

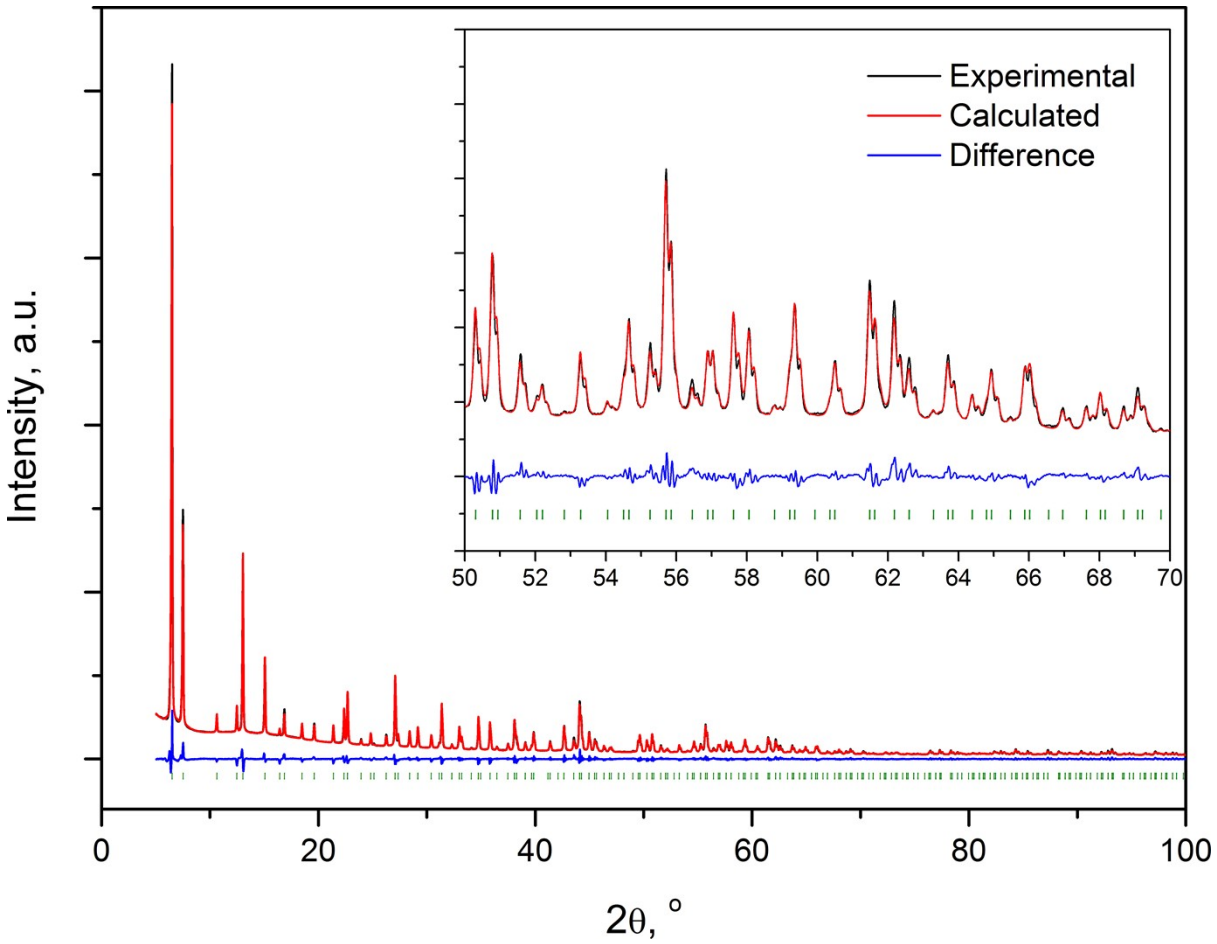

Fig. S4 The Rietveld profile fitting for **1** (the green bars represent the calculated positions for the peak positions).

The Rietveld refinement concludes with a reasonably good R value of R = 0.0315, however with a relatively high goodness of fit, GoF = 5.9. The latter is in a significant part due to the non-corrected instrumental factor: the asymmetry of the first two peaks were not possible to fit precisely by standard procedures (a manual adjustment of the background was not used as the procedure could be viewed as a dubious practice in this case).

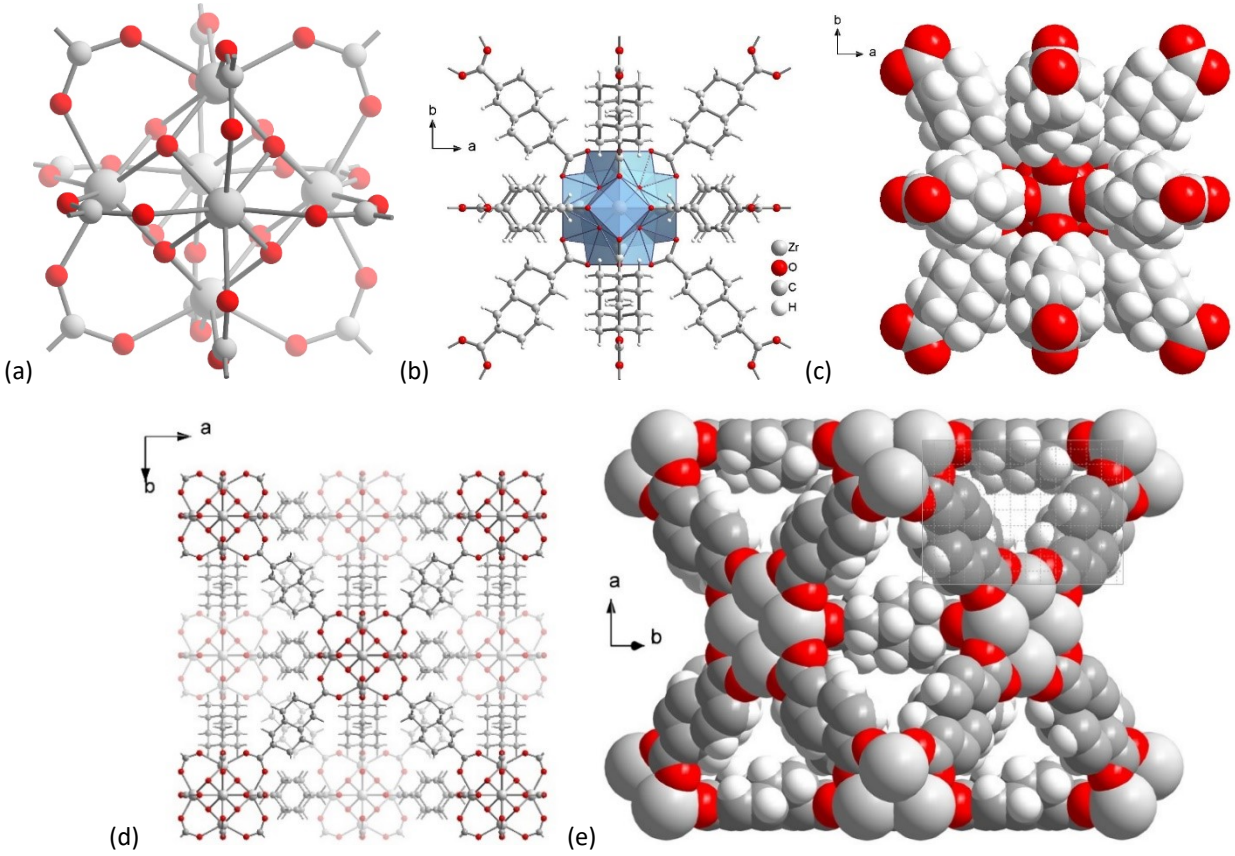

Fig. S5 a-c) Different views on the {Zr_6} cluster; note the very small exposed surface of the inorganic cluster-core on the last image; d) the framework structure of **1**; e) a representative fragment demonstrating the size of the pore entrances (an Angström-net overlay is shown in the top right corner).

The structural fragments are shown in lowered Fm$\bar{3}$ symmetry, without disorder. The positions of the oxygen atoms of the μ_3-OH/O groups are represented by one merged atom for simplicity.

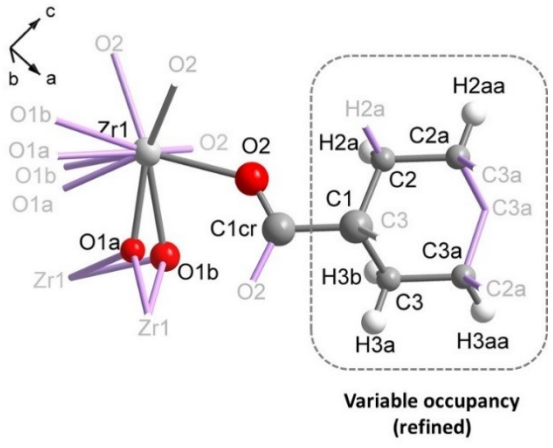

Fig. S6 The asymmetric unit of **1**, with the bonds to the symmetry equivalents shown in light-violet (the atomic radii correspond to thermal displacements set at 50% probability). The positions of the O atoms belonging to the site-sharing μ_3-O/OH ligands were refined separately (on other images their merged position is shown for simplicity)

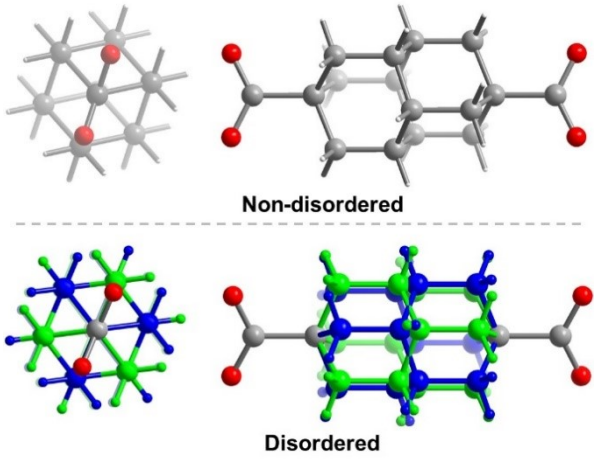

Fig. S7 The non-disordered adamantane-4,9-dicarboxylate *vs* the disordered linker in the structure of **1**. The two-positional disorder relates the components through a center of inversion. The diamantane moiety has D_{3d} symmetry, while the disordered moiety has D_{6h} symmetry. The second case is compatible with the m.mm site symmetry of the respective 'ligand'-site in the UiO-66 type structure with the highest Fm$\bar{3}$m symmetry

S3 Infrared spectroscopy

The Fourier transform infrared (FT-IR) spectra were collected with a Bruker Tensor 37 instrument on samples dispersed in KBr pellets in the range of 4000-400 cm^{-1} (Fig. S8). In the region between 3700 and 3200 cm^{-1} the broad absorption band is related to the stretching vibration of O-H bond of adsorbed water within the framework.[7] The band at 2874 cm^{-1} is assigned to the C-H stretching vibration of the diamantane core of the ligand. The bands at 1570 and 1432 cm^{-1} are assigned to the carboxylate group: the band at 1570 cm^{-1} corresponds to asymmetric stretching and 1432 cm^{-1} to symmetric stretching. The band at 672 cm^{-1} corresponds to the stretching of O-Zr-O bonds.[8] The band at 455 cm^{-1} is related to the in-plane and out-of-plane bending vibration of the carboxylate group.

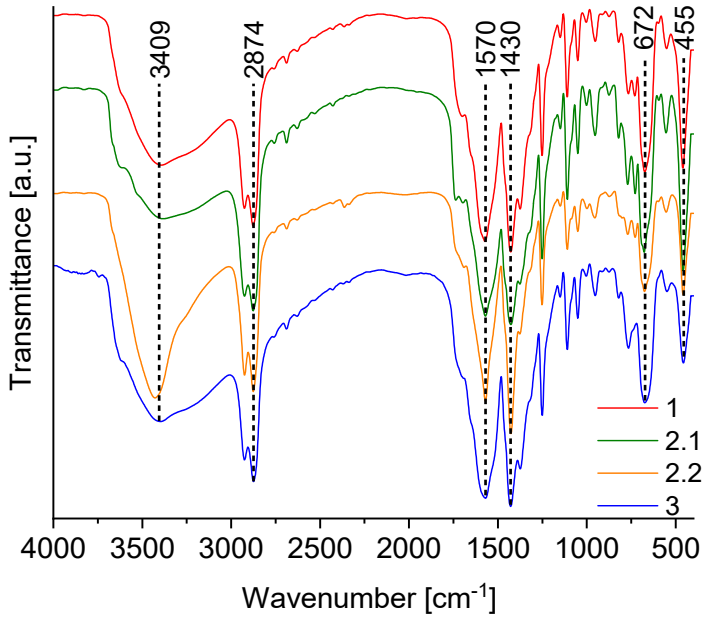

Fig. S8 Fourier transform infrared spectra (FT-IR) of the HHUD-3 samples **1**, **2.1**, **2.2** and **3**.

S4 Thermogravimetric analysis, TGA

The thermogravimetric analysis was carried out on a Netzsch TG 209 F3 Tarsus instrument (heating rate of 5 °C min^{-1}) using an aluminium oxide sample holder under synthetic air atmosphere (80% N_2 / 20% O_2) with a gas stream of 10 mL min^{-1}. Prior to TGA, the samples were dried under reduced pressure at 140 °C (413 K), assuming an analogue with other Zr-MOFs, particularly UiO-66, where the desorption of physisorbed water molecules from the pores of the compound typically occurs at temperatures below 150°C.[9,10]

The obtained TGA curves (Fig. S9) show the thermal decomposition of the investigated compounds. The TGA curves in Fig. S9a are normalized to 100% of the initial relative weight of the samples, while in Fig. S9b the same curves are normalized to 100% final weight of the residue after the oxidative decomposition. The TGA curves show no or only a slight mass loss in the temperature range up to 150 °C, due to the sample preparation, which removes the major part of the guest molecules. The next step of weight-loss, starting at 200 °C, can be, at least partially, related to the dehydroxylation of the zirconium hydroxido-oxido-clusters $\{Zr_6O_4(OH)_4\}$ to give $\{Zr_6O_6\}$.[9,10] The latter process continues for UiO-66 and UiO-67 to about 350 °C. A minor amount of solvents trapped during the synthesis in isolated solvent-inaccessible pockets (associated with defect-free parts of the structure), could also be released at temperatures beyond 200 °C. The steep weight-loss above 250 °C can only be associated to the oxidative decomposition of the structure, eventually leaving ZrO_2 as the only residue. Thus, the decomposition in HHUD-3 above 250 °C overlaps with the dehydroxylation in the TGA plot, in the range of 150-250 °C. In any case the impact of the weight loss due to dehydroxylation is small (< 1.5% for two H_2O molecules) in order to substantially affecting the precision of the defect determination.

The calculation of the number of missing-linker defects based on the actual MOF formula was performed without accounting for the dehydroxylation process, which overlaps with decomposition. Accordingly the relative experimental "plateau" weight, $W_{exp.\,Plat.}$, referring to the degassed, but not dehydroxylated material, is taken at 150 °C (the majority of the DMF guest molecules is removed during the sample preparation, which is also corroborated by the nearly unchanged surface areas registered for degassing at higher temperatures; see Section S6, p. 12).

$$[Zr_6O_4(OH)_4(C_{16}H_{18}O_4)_6] + 114\ O_2 \xrightarrow{> \sim 150\ ^\circ C} 6\ ZrO_2 + 96\ CO_2 + 56\ H_2O$$

The calculation of the number of defects was done similarly to the calculation by Shearer *et al.,* albeit using a reference point taken at lower temperature, corresponding to the non-dehydroxylated formula.[11] It is assumed that a complete decomposition of the samples occurs, with ZrO_2 remaining as the only residue. The approach, used because the weight associated with the dehydroxylated compound cannot be determined, is an approximation, which gives a low estimate for the number of defects (it does not account for the presence of terminal ligands which substitute the linkers, either formates or OH/OH_2, as well as for the minor amounts of residual solvent molecules trapped in the non-accessible pores. Accounting for the linker-substituting ligands gives even higher amount of defects, which might suggest the presence of unaccounted Zr-rich species. Due to the limited knowledge regarding the types of actual defects and additional species present, we report a formal lower estimate, using a methodology standard for UiO-66. In any case, the problematics of defects in UiO-66 analogues based on bulky ligands is a topic deserving dedicated attention).

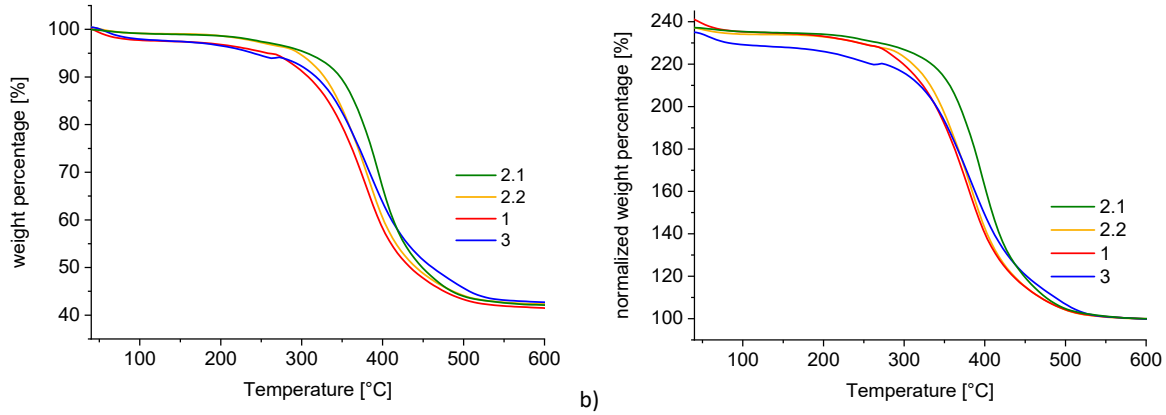

a) b)

Fig. S9 TGA curves of HHUD-3 samples **1**, **2.1**, **2.2** and **3,** normalized such that the initial weight is 100% (a) and the final weight is 100% (b).

The calculation of the missing linker defects was carried out as follows:

Determination of the theoretical TGA plateau

The theoretical TGA plateau $W_{theo.\,Plat.}$ can be calculated according to the reaction equation from above.

$$W_{theo.\,Plat.} = \frac{M_{MOF\,theo.}}{M_{6xZrO_2}} \bullet W_{fin.} \qquad (1)$$

$W_{theo.\,Plat.}$: weight percent theoretical TGA plateau

$M_{MOF\,theo.}$: molar weight of the defect-free MOF composition, here $[Zr_6O_4(OH)_4(C_{16}H_{18}O_4)_6]$ (no dehydroxylation)

M_{6xZrO_2}: six times the molar weight of ZrO_2 (739.34 g/mol)

$W_{fin.}$: Final weight percent after TGA normalization (100%)

$M_{MOF\,theo.}([Zr_6O_4(OH)_4(C_{16}H_{18}O_4)_6]) = 2325\ \mathrm{g/mol}$

This results in the following values for the calculation of the theoretical TGA plateau

$W_{theo.\,Plat.}([Zr_6O_4(OH)_4(C_{16}H_{18}O_4)_6]) = 314.5\%$

The average percentage weight contribution per linker $Wt.\,pL_{theo.}$ ***to the weight percent theoretical TGA plateau,*** $W_{theo.Plat.}$

$$Wt.\,pL_{theo.} = \frac{W_{theo.\,Plat.} - W_{fin.} + Corr.\,factor}{NL_{ideal}} \qquad (2)$$

NL_{ideal}: ideal number of Linker per SBU: 6

Since 6 times the molar weight of ZrO_2 is not equal to the molar weight of $Zr_6O_4(OH)_4$, a correction factor $Corr.\ factor$ was used to calculate $Wt.\ pL_{theo.}$

$$Corr.\ factor = \frac{M_{6xZrO_2} - M_{Zr_6O_4(OH)_4}}{M_{6xZrO_2}} \bullet 100\% = 8.1\% \quad (3)$$

$$Wt.\ pL_{theo.}\ ([Zr_6O_4(OH)_4(C_{16}H_{18}O_4)_6]) = 37.1\%$$

The number of linkers per Zr_6-formula unit and the number of defects per Zr_6-formula unit ($[Zr_6O_4(OH)_4(C_{16}H_{18}O_4)_6]$).

The experimentally determined number of linkers per Zr_6-formula unit can be determined using the following formula.

$W_{exp.\ Plat.}$: experimental TGA plateau. The value of the experimental TGA plateau before the decomposition of the compound was determined from the TGA plots of the respective samples in the Fig. S9b at the temperature value of 150 °C.

$$NL = 6 - X = \frac{W_{exp.\ Plat.} - W_{fin.} + Corr.\ factor}{Wt.\ pL_{theo.}} \quad (4)$$

X is the number of defects, i.e. missing linkers per Zr_6-formula unit and can be determined by rearranging the formula (3).

$$X = 6 - NL = 6 - \left(\frac{W_{exp.\ Plat.} - W_{fin.} + Corr.\ factor}{Wt.\ pL_{theo.}}\right) \quad (5)$$

The calculated data of the samples are put into the formula (4).

$$X = 6 - NL = 6 - \left(\frac{W_{exp.\ Plat.} - 100\% + 8.1\%}{35.8\%}\right) \quad (6)$$

The following Table S3 shows the determined values of the $W_{exp.\ Plat.}$ and the calculated number of defects per Zr_6-formula unit X by using the formula (6).

Table S3 Calculated number of defects per Zr_6 formula unit in HHUD-3

Sample	$W_{exp.\ Plat.}$ [%]	Number of missing ligand defects per Zr_6 formula unit X
1	235	2.14
2.1	235	2.14
2.2	234	2.17
3	228	2.33

The found number of defects (more specifically the number of missing linkers) in the Zr_6-formula unit of the respective samples were always slightly more than 2, which is considered to be the reasonable maximum of defects, which still ensures enough mechanical stability. This result might be related to the sterics of the ligand and also due to relatively low temperature (120 °C) using formic acid as a modulator (typically, the number of defects decreases with temperature, and the defect free UiO-66 could only be synthesized at high temperatures, whereas syntheses at low temperatures with acids as modulators lead to more defects).[12] The rather high number of missing linker defects in the HHUD-3 samples, relative to other UiO compounds, is reflected in the lower thermal stability of HHUD-3 compared to other UiO compounds (with the partial exception of the highly defected case of HCl-modulated structure).

The sample **3** has an appreciable larger number of defects, ~2.3, compared to other samples with ~2.15 defects. This result is also consistent with the PXRD data of sample **3**, as it shows lower crystallinity or larger strain, which can be partially attributed to the increased number of defects.

S5 Calculated surface areas and void volumes

Table S4 Calculated surface areas and void volumes of HHUD-3 **1**: $Zr(OH)_4(O)_4L_6$, non-defected; **1-4FA**: $Zr(OH)_4(O)_4L_4(HCOO)_4$, four regularized missing-linker defect model (**bcu** topology), with the missing linkers positions occupied by formates.

[a]	NonorthoSA		Zeo++		Mercury	
	1	**1-4FA**	**1**	**1-4FA**	**1**	**1-4FA**
Total surf. Area [m^2g^{-1}]	787	1693	918	1854		
Accessible surf. area [max. pocket surf area], [m^2g^{-1}]			0	1854		
Pore volume, [cm^3g^{-1}]			0.082	0.169	0.074 [0.384] [b]	0.155 [0.530] [b]

[a] Software used: NonorthoSA [13] Zeo++ [14] and by Mercury[15]

[b] Pore volume fractions calculated with 'solvent accessible-' and ['contact surface'] parameters as defined in Mercury[15] (probe radius: 1.82 Å, grid 0.1 Å). The 'solvent accessible' parameter in this case does not distinguishes between accessible and pocket pores, but it correctly describes the volume, which can be occupied by the centre of a probe of a given radius. The contact surface parameter, which stipulates a calculation of a probe-rolling surface, see, e.g. [16], gives rather the profile of the pore surface and overestimates the porosity as does not check for overlap with neighbouring surfaces (the value is given to reflect the intricate narrow-pore system with a developed surface-area, which becomes gradually accessible upon decrease of the probe size).

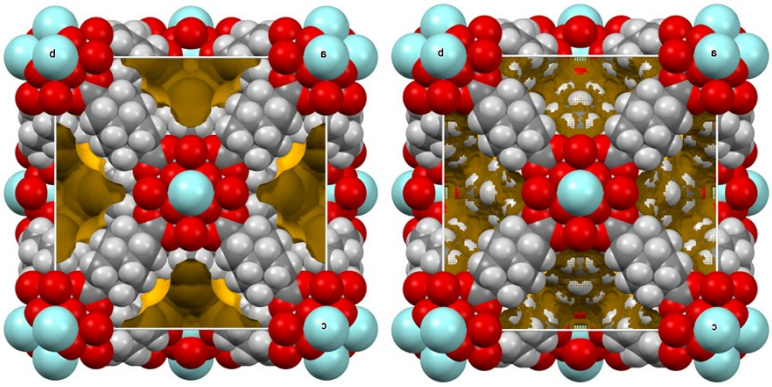

Fig. S10. Pore profiles (solvent accessible surface area on the left and contact surface area on the right) for **1** as computed by the Voids procedure in Mercury.[15] All pores are represented by pockets, non-accessible by solvent molecules of the size of, at least equal or above, water with a size of ~2.4 Å

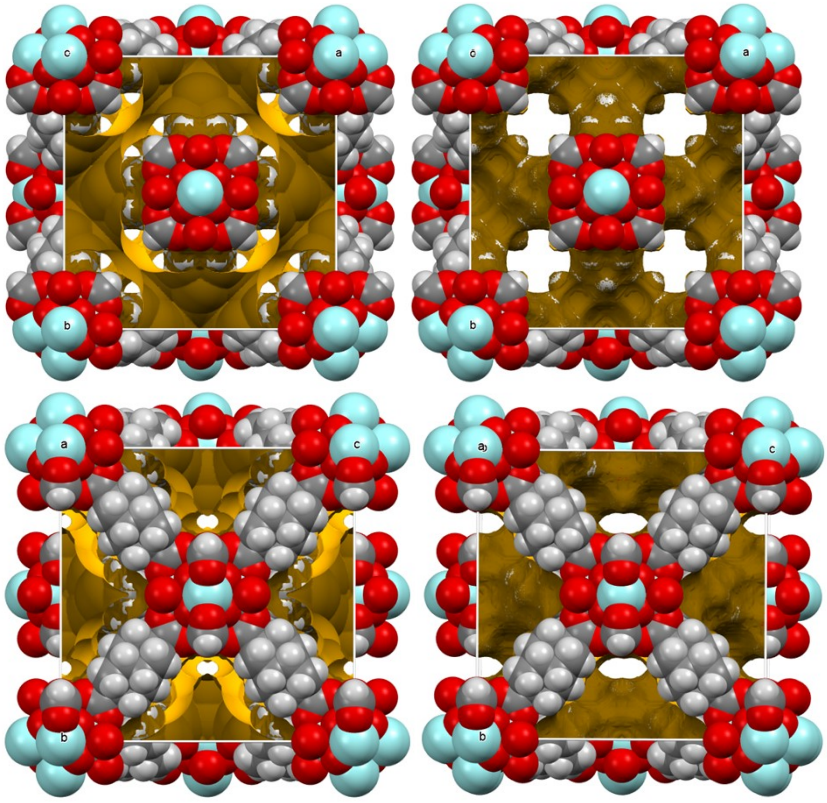

Fig. S11. Pore profiles (solvent accessible surface area on the left and contact surface area on the right) for the **1-4FA** model with four regularized defects represented by formates (**bcu** topology) as computed by the Voids procedure in Mercury.[15]

S6 Gas adsorption studies

All used gases were of ultrapure purity grades (>99.999%). Before each experiment the samples were activated via heating at 413 K for 16 h under reduced pressure < 10^{-3} mbar. (Since the TGA measurements of the activated samples, which were prior washed with ethanol, showed no evidence of significant amounts of DMF in the samples, the activation temperature of 413 K was kept, as higher temperatures could have a negative influence on the crystallinity of frameworks with a high number of defects.)

The N_2 adsorption isotherms were measured using the Quantachrome Autosorb IQ MP and a Quantachrome Autosorb 6 gas sorption analyzer. The measurements were carried out at 77 K.

The argon sorption isotherms were collected by the Quantachrome Autosorb IQ MP. The measurements were carried out at 87 K by using a Quantachrome cryocooler to adjust the temperature.

The carbon dioxide sorption measurements were performed by the Quantachrome Autosorb IQ MP at 273 K within a pressure range of 2 x 10^{-4} to 0.96 bar.

Hydrogen sorption measurements were performed by a Quantachrome Autosorb IQ MP at 77 K within a pressure range of 9.5 x 10^{-5} to 0.96 bar.

Methane sorption measurements were performed by the Quantachrome Autosorb IQ MP at 273 K within a pressure range of 1.5 x 10^{-4} to 0.96 bar.

For further characterization of the synthesised compounds, sorption measurements were carried out with N_2, Ar, CO_2, H_2, and CH_4. The surface area and the porosity characteristics of the compounds were calculated using the sorption data of N_2 and Ar with the sorption isotherms being shown in Fig. S12. The surface area was determined using the BET method and the results are summarized in Table S5. The surface area difference obtained from Ar and N_2 sorption is recognisable in all samples. Due to the quadrupole moment of the nitrogen molecule the interaction of nitrogen depends on the surface chemistry of the porous compound and leads to different amounts of space being occupied on the surface. Argon on the other hand does not have a quadrupole moment, its atoms always require the same amount of space on the surface of an adsorbent.[17] From the data of König et al.[18] it is evident that the BET surfaces of studied MOFs differ depending on the adsorptive being used, whereby all values determined by nitrogen sorption are higher than the values determined with argon.

The sorption isotherms in the nitrogen and argon sorption measurements of **1** are type Ib isotherms, which overall indicates a microporous material. In both cases, a slight type H3 hysteresis is visible. That can be explained by a small proportion of narrow mesopores and aggregated crystals within a microporous compound. A similar result can be observed in the sorption isotherms of **2.1**, with a type Ia isotherm in the nitrogen sorption measurement and a type Ib isotherm in the argon sorption measurement. However, there is no hysteresis in either isotherm, which indicates minimal mesoporosity and textural effects arising from aggregation of crystals. The difference between **2.1** and **2.2** is a slight hysteresis (H3) in the sorption isotherms of compound **2.2**. As with **1** that indicates a low proportion of mesopores and aggregated crystals. The sorption isotherms of **3** (N_2 and Ar) show a clear difference to the samples **1**, **2.1** and **2.2**. Both isotherms are type IV(a) isotherms and demonstrate a strong hysteresis (type H2). The shape of the sorption isotherms with the occurring hysteresis is characteristic of mesoporous compound and can be explained by the capillary condensation of the absorbed gas. The shape of the hysteresis with its smoothly increasing adsorption branch and the relatively steep desorption branch indicates complex pore structures, where pore openings have narrow spots and therefore a much smaller diameter than the pore itself (ink-bottle-type pores).[19]

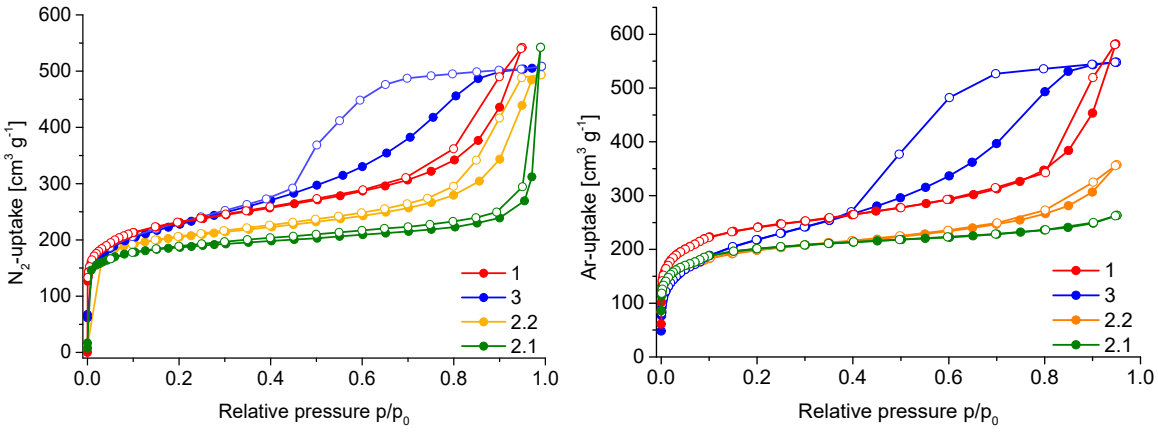

Fig. S12. Nitrogen (left) and argon (right) sorption isotherms of HHUD-3 samples **1**, **2.1**, **2.2** and **3** measured at 77 K and 87 K respectively (adsorption filled, desorption empty symbols).

Table S5. Results of sorption analysis for the HHUD-3 samples calculated from N_2, Ar, CO_2, CH_4 and H_2 adsorption isotherms.

Samples	S_{BET} [m^2g^{-1}] N_2 ads.	Micropore volume [cm^3g^{-1}] N_2 ads.	S_{BET} [m^2g^{-1}] Ar ads.	Micropore volume [cm^3g^{-1}] Ar ads.	CO_2 uptake 273 K 0.96 bar [mmol g^{-1}]	CH_4 uptake at 273 K and 0.96 bar [mmol g^{-1}]	H_2 uptake at 77 K and 0.96 bar [mmol g^{-1}]
1	869	0.244	811	0.211	1.829	0.977	5.779
2.1	716	0.247	685	0.227	2.201		
2.2	781	0.239	667	0.193	1.933		
3	832	0.120	713	0.055	1.936		

Comparing the results of the calculated BET surface areas of the samples, it can be seen that the surface area values of **2.1** and **2.2** are the lowest and are in a similar range (**2.1**: N_2–S_{BET} = 718 m^2g^{-1}, Ar–S_{BET} = 685 m^2g^{-1}; **2.2** N_2–S_{BET}= 781 m^2g^{-1}, Ar–S_{BET} = 667 m^2g^{-1}). This similarity can be explained by the fact that the synthesis conditions of these samples were identical and only the Zr-source was different. Sample **3** has higher S_{BET} with N_2–S_{BET} = 832 m^2g^{-1} and Ar–S_{BET} = 713 m^2g^{-1} than **2.1** and **2.2**. With N_2–S_{BET} = 869 m^2g^{-1} and Ar–S_{BET} = 811 m^2g^{-1} **1** has the highest S_{BET} – values of all samples.

The differences between the samples can be explained by the different synthesis conditions. Comparing samples **2.1**/**2.2** and **1**, the higher surface area of **1** can be due to different metal to linker ratios. While the molar zirconium to linker ratio (Zr:H_2L) of 3 to 8 was used in samples **2.1**/**2.2** (the linker was used in excess), the Zr:H_2L in sample **1** was almost equimolar at 7 to 8. The higher relative amount of linker in **2.1**/**2.2** may lead to the trapping of the excess ligand in the pores, causing a reduction in the surface area of the compound. In comparison to **2.1/2.2**, the Zr:H_2L ratio of 3 to 4 and doubled concentration of the ligand was used in **3**, however, the result is quite different. The characteristics of the adsorption isotherm observed for **3** witnesses both mesoporosity and macroporosity, which complements the observation of a higher number of defects on the level of the SBU, as witnessed by the TGA.

Pore size calculations based on non-local density functional theory (NLDFT) show that for samples **1, 2.1**, and **2.2** the majority of the pores are in the microporous range with a diameter less than 20 Å (Fig. S13). However, it can be seen that sample **3** also has a significant fraction of pores in the mesoporous region, with a pore size of 33 Å. This corresponds well with the character of the sorption isotherms of **3**, which shows a clear hysteresis, indicating the presence of mesopores in the network.

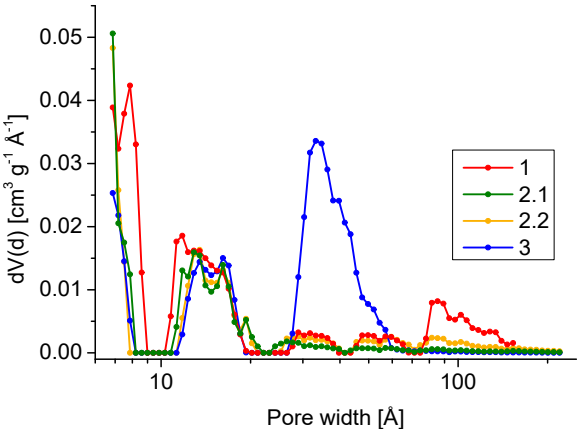

Fig. S13 Pore size-distribution of HHUD-3 samples **1**, **2.1**, **2.2**, and **3** determined from Ar sorption at 87 K, calculated using the NLDFT equilibrium model.

The CO_2 uptake of the samples was determined according to the isotherms shown in Fig. S14 and the data are included in Table S5. The measured values of all samples at 0.96 bar differ only slightly.

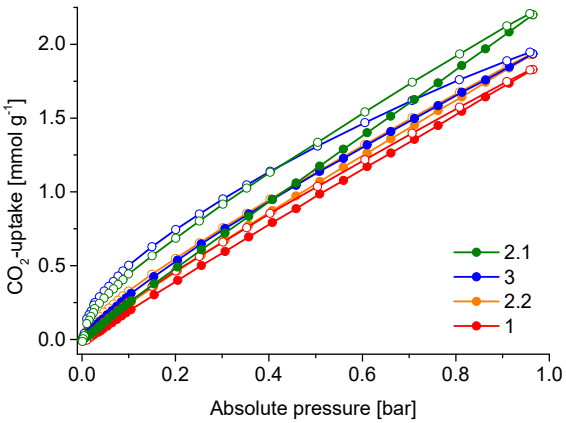

Fig. S14 CO_2 sorption isotherms of HHUD-3 samples **1**, **2.1**, **2.2**, and **3** measured at 273 K (adsorption filled, desorption empty symbols).

Nitrogen sorption measurements of HHUD-3 **1** were carried out with the sample activated at temperatures of 140 °C, 180 °C, and 220 °C with the following results for the surface area: 140 °C - S_{BET} = 869 m^2g^{-1}; 180 °C - S_{BET} = 849 m^2g^{-1}; 220 °C - S_{BET} = 874 m^2g^{-1}. Based on the sorption isotherms (Fig. S15) and the calculated surface area, it is evident that the activation temperature of 140 °C is sufficient, as higher activation temperature does not influence the uptakes significantly.

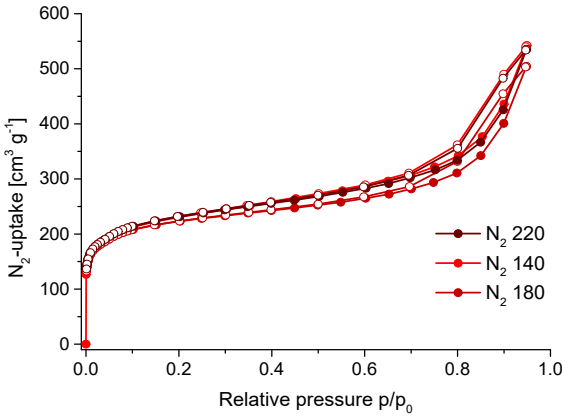

Fig. S15 Nitrogen sorption isotherms of HHUD-3 **1** for activation temperatures of 140 °C, 180 °C, and 220 °C (adsorption filled, desorption empty symbols).

References

1 L. Valenzano, B. Civalleri, S. Chavan, S. Bordiga, M. H. Nilsen, S. Jakobsen, K. P. Lillerud and C. Lamberti, *Chem. Mater.*, 2011, **23**, 1700.
2 G. Nickerl, M. Leistner, S. Helten, V. Bon, I. Senkovska and S. Kaskel, *Inorg. Chem. Front.*, 2014, **1**, 325.
3 B. H. Toby and R. B. Von Dreele, *J. Appl. Crystallogr.*, 2013, **46**, 544.
4 M. J. Cliffe, W. Wan, X. Zou, P. A. Chater, A. K. Kleppe, M. G. Tucker, H. Wilhelm, N. P. Funnell, F.-X. Coudert and A. L. Goodwin, *Nat. Commun.*, 2014, **5**, 4176.
5 V. Petříček, M. Dušek and L. Palatinus, *Zeitschrift für Krist. – Cryst. Mater.*, 2014, **229**, 345.
6 B. H. Toby, *Powder Diffr.*, 2006, **21**, 67.
7 K. A. Mocniak, I. Kubajewska, D. E. M. Spillane, G. R. Williams and R. E. Morris, *RSC Adv.*, 2015, **5**, 83648.
8 M. A. Rodrigues, J. d. S. Ribeiro, E. d. S. Costa, J. L. d. Miranda and H. C. Ferraz, *Sep. Purif. Technol.*, 2018, **192**, 491.
9 H. N. Abdelhamid, *Dalton Trans.*, 2020, **49**, 10851.
10 Q. Yang, H.-Y. Zhang, L. Wang, Y. Zhang and J. Zhao, *ACS Omega*, 2018, **3**, 4199.
11 G. C. Shearer, S. Chavan, S. Bordiga, S. Svelle, U. Olsbye and K. P. Lillerud, *Chem. Mater.*, 2016, **28**, 3749.
12 G. C. Shearer, S. Chavan, J. Ethiraj, J. G. Vitillo, S. Svelle, U. Olsbye, C. Lamberti, S. Bordiga and K. P. Lillerud, *Chem. Mater.*, 2014, **26**, 4068.
13 T. Düren, F. Millange, G. Férey, K. S. Walton and R. Q. Snurr, *J. Phys. Chem. C*, 2007, **111**, 15350.
14 T. F. Willems, C. H. Rycroft, M. Kazi, J. C. Meza and M. Haranczyk, *Microporous Mesoporous Mater.*, 2012, **149**, 134.
15 C. F. Macrae, I. Sovago, S. J. Cottrell, P. T. A. Galek, P. McCabe, E. Pidcock, M. Platings, G. P. Shields, J. S. Stevens, M. Towler and P. A. Wood, *J. Appl. Cryst.*, 2002, **53**, 226.
16 L. J. Barbour, *Chem. Commun.*, 2006, 1163.

17 M. Thommes, K. Kaneko, A. V. Neimark, J. P. Olivier, F. Rodriguez-Reinoso, J. Rouquerol and K. S. W. Sing, *Pure Appl. Chem.*, 2015, **87**, 1051.
18 S. König, J. B. Mietner, K. Peikert, M. Rogaczewski, F. Brieler and M. Fröba, *Quantachrome Partikelwelt*, 2016, **17**, 16.
19 K. Morishige, N. Tateishi, *J. Chem. Phys.*, 2003**, 119**, 2301.